J|A|C|S ARTICLES

Published on Web 01/27/2010

Structure-Relaxation Interplay of a New Nanostructured Membrane Based on Tetraethylammonium Trifluoromethanesulfonate Ionic Liquid and Neutralized Nafion 117 for High-Temperature Fuel Cells

Vito Di Noto,*[,†,‡] Enrico Negro,[†,‡] Jean-Yves Sanchez,[§] and Christina Iojoiu[§]

Dipartimento di Scienze Chimiche, Università di Padova, Via Marzolo 1, I-35131 Padova (PD), Italy, Istituto di Scienze e Tecnologie Molecolari, ISTM-CNR and INSTM, Dipartimento di Scienze Chimiche, Via Marzolo 1, I-35131 Padova (PD) Italy, and LEPMI, Laboratoire d'Electrochimie et de Physico-chimie des Matériaux et des Interfaces, UMR 5631 CNRS-INPG, 1130 Rue de la Piscine, associée à l'UJF, ENSEEG B.P.75. 38402 Saint-Martin-d'Héres, Cedex, France

Received August 20, 2009; E-mail: vito.dinoto@unipd.it

Abstract: In this report, the electrical performance at $T > 100$ °C and low relative humidity of proton-conducting Nafion-based membranes was improved by preparing new materials based on Nafion 117 (N117) neutralized with triethylammonium (TEA^+) and doped with the ionic liquid (IL) trifluoromethanesulfonate of triethylammonium (TEA-TF). In particular, a new two-step protocol for the preparation of $[N117^{x-}(TEA^+)_x/(TEA\text{-}TF)_y]$ is proposed. $[N117^{x-}(TEA^+)_x/(TEA\text{-}TF)_y]$ membrane is composed of ca. 30 wt % of TEA-TF. The structure of the different nanophases composing the materials and their interactions were investigated by FT-IR ATR and micro-Raman spectroscopy. The thermal stability, water uptake, and mechanical properties of the membranes were studied by thermogravimetric analysis and dynamic mechanical analysis measurements. With respect to pristine N117, the thermal and mechanical properties of the proposed materials were improved. The electric response of $[N117^{x-}(TEA^+)_x/(TEA\text{-}TF)_y]$ was studied by broad band dielectric spectroscopy in the frequency range from 10^{-2} Hz to 10 MHz and for temperatures between 5 and 155 °C. In comparison to the N117 reference, the following was observed: (a) the stability range of conductivity (SRC) of the $[N117^{x-}(TEA^+)_x]$ membrane increases up to 155 °C, while its σ_{DC} at $T = 100$ °C is lowered by ca. 2 orders of magnitude; (b) the SRC of $[N117^{x-}(TEA^+)_x/(TEA\text{-}TF)_y]$ is similar to that of $[N117^{x-}(TEA^+)_x]$, while the σ_{DC} at 145 °C decreases in the order $7.3 \times 10^{-3} > 6.1 \times 10^{-3} > 9.7 \times 10^{-4}$ $S \cdot cm^{-1}$ for $[N117^{x-}(TEA^+)_x/(TEA\text{-}TF)_y]$, N117, and $[N117^{x-}(TEA^+)_x]$ membranes, respectively. In conclusion, the lower water uptake, the improved thermal and mechanical stability, and the good conductivity make $[N117^{x-}(TEA^+)_x/(TEA\text{-}TF)_y]$ a promising membrane to improve for application in proton exchange membrane fuel cells operating under anhydrous conditions at $T > 100$ °C.

1. Introduction

Proton exchange membrane fuel cells (PEMFCs) are electrochemical devices for the conversion of chemical energy into electrical power characterized by a high efficiency and a low environmental impact.[1] PEMFCs can be used in a variety of applications ranging from cellular phones to small stationary power plants; indeed, PEMFCs are easily scalable and show a very large energy density.[2] PEMFCs are also the fuel cells of choice for application in the automotive field.[3] Nowadays, perfluorinated polymer electrolytes such as Nafion, Aciplex, Flemion and Dow membranes are the most promising membranes for application in PEMFCs operating at temperatures lower than 100 °C.[4] Even if these perfluorinated systems are characterized by good chemical stability and good proton conductivity, their performance is strongly dependent on their hydration degree and becomes very poor over 90 °C and at a low relative humidity.[4,5] In addition, these materials are very expensive. All these drawbacks limit the large-scale commercial application of the modern perfluorinated ionomers. The development of PEMFCs operating above 120 °C in dry conditions is a significant milestone to be reached in the quest to devise a feasible fuel cell car. Such a PEMFC does not require humidification subsystems, the thermal management of the device is much easier, and the issue of CO poisoning on the electrocata-

[†] Università di Padova.
[‡] ISTM-CNR and INSTM.
[§] LEPMI.

(1) O'Hayre, R.; Cha, S. W.; Printz, F. B. *Fuel Cell Fundamentals*; John Wiley & Sons: Hoboken, NJ, 2006; p 8.
(2) Vielstich, W. In *Handbook of Fuel Cells - Fundamentals, Technology and Applications*; Vielstich, W., Lamm, A., Gasteiger, H. A., Eds.; Wiley: Chichester, 2003; Vol. 1, p 26.
(3) Lamm, A.; Müller, J. In *Handbook of Fuel Cells - Fundamentals, Technology and Applications*; Vielstich, W., Lamm, A., Gasteiger, H. A., Eds.; Wiley: Chichester, 2003; Vol. 4, p 878.
(4) Grot, W. *Fluorinated Ionomers*; William Andrew Publishing: Norwich, 2008.
(5) Vielstich, W.; Lamm, A.; Gasteiger, H. A. *Handbook of Fuel Cells - Fundamentals, Technology and Applications*; Wiley: Chichester, 2003; Vol. 3.

lysts can be successfully addressed.[6,7] One possible approach to solve this drawback is to use anhydrous proton conductors such as blends of polybenzimidazole and phosphoric acids as proposed by Fontanella et al.[8] Recently, it was reported that perfluorinated membranes containing proton-conducting ionic liquids (PCILs) are promising systems to address these issues owing to their good ionic conductivity under anhydrous conditions.[9] PCILs are salts which are liquid at room temperature and consist of a bulky, asymmetric organic cation and an inorganic anion.[10] PCILs are characterized by a wide electrochemical window, high ionic conductivity, and high thermal stability.[10−12] One way to obtain an anhydrous proton-conducting membrane consists of hosting PCILs in a high-performance nonionic matrix such as the fluorinated copolymer of vinylidene fluoride and hexafluoropropene PVdF-HFP.[13] However, conductivities lower than 10^{-2} S·cm^{-1}, i.e. clearly lower than that of pristine PCILs, have been observed for PVdF-HFP/PCIL blends. In addition, the PVdF-HFP copolymer has a melting point close to 150 °C and is characterized by a lower crystallinity if compared with the PVdF homopolymer. Thus, the thermomechanical properties of the PVdF-HFP/PCIL membrane resulted in being inadequate for application in PEMFCs. It was proposed that Nafion membranes can be used in PEMFCs operating at $T > 100$ °C and low RH% when this ionomer is impregnated with PCILs.[14] Indeed, conductivities of 1.2×10^{-3} S·cm^{-1} at 125 °C and 5.1×10^{-3} S·cm^{-1} at 150 °C were measured with Nafion membranes impregnated respectively with 1-ethyl-3-methyl-imidazolium triflate (EMI-TF)[15] and 1-butyl-3-methyl-imidazolium triflate (BMI-TF).[14] In this latter case, the membrane was doped with 32 wt % of BMI-TF. Different ion conductors based on Nafion impregnated with both hydrophilic and hydrophobic ILs were investigated,[16] suggesting the following: (a) the conductivity of impregnated Nafion membranes increases with the size of the counterion and the amount of adsorbed IL; (b) the interaction of the IL with the hydrophobic domains and the hydrophilic clusters of pristine Nafion results in a homogenization of the polymer host owing to the collapse of ionic cluster structures and their interconnecting pathways. It was reported that the IL uptake depends on the nature of the IL anion, while IL washing out from bulk membranes is regulated by IL hydrophilicity. In addition, Schmidt et al. claimed that ILs act as "potent" plasticizers for the Nafion membrane, greatly reducing its elastic module and resulting in higher breaking strains.[16] Other works report the properties of new PCILs obtained by reacting several amine derivatives with perfluorinated acids.[17,18] The main advantages of these PCILs arise from their anhydrous proton conductivity and from their high thermal stability. Thus, it is expected that membranes for application in PEMFCs operating above 120 °C in dry conditions can be obtained by doping Nafion with these latter PCILs. The aim of this report was to improve the electrical performance of Nafion-based membranes at $T > 100$ °C and low RH% by preparing new [N117/(IL)$_y$] materials where IL = trifluoromethanesulfonate of triethylammonium (TEA-TF). In particular, a new two-step protocol for the preparation of the [N117^{x-}(TEA$^+$)$_x$/(TEA-TF)$_y$] material is proposed. First, an N117 membrane in acid form is reacted with triethylamine to obtain a neutralized [N117^{x-}(TEA$^+$)$_x$]. With respect to the acid form, [N117^{x-}(TEA$^+$)$_x$] is expected to be characterized by (a) a larger SRC and (b) a lower proton conductivity.[5] Second, with the aim to raise the σ_{DC} of the membranes, [N117^{x-}(TEA$^+$)$_x$] was doped with TEA-TF, a good proton-conducting ionic liquid.[17,18] This latter step was carried out by adsorbing TEA-TF into [N117^{x-}(TEA$^+$)$_x$]. The structure and the interactions between the different components were investigated by FT-IR ATR spectroscopy. The thermal stability, water uptake (W.U.), and mechanical properties of the membranes were analyzed by thermogravimetric analysis (TGA) and dynamic mechanical analysis (DMA). The electric response of prepared materials was investigated by BDS spectroscopy in the frequency range from 10^{-2} Hz to 10 MHz and for temperatures ranging from −155 to 155 °C.

2. Experimental Section

2.1. TEA-TF Synthesis. The TEA-TF synthesis was carried out in doubly distilled water by reacting trifluoromethanesulfonic acid with freshly distilled triethylamine. The aqueous solution was then filtered on a carbon active column, and water was removed by evaporation. The resulting proton-conducting ionic liquid (TEA-TF) was dried for 48 h at 130 °C under vacuum. PCIL purity was then checked by elemental analysis and by NMR, using a Bruker WM 250 spectrometer operating at frequencies of 250 MHz for the protons and 230 MHz for ^{19}F. The samples were dissolved in $CDCl_3$. The peak assignment of TEA-TF was made by reference to the starting amines and acids. The traces of water in the PCIL were determined by the Karl Fischer method and resulted in ∼0.05 wt %. Thus, the purity of TEA-TF was 99.95%.

2.2. Membrane Preparation. First, the N117 membrane was modified by neutralization with triethylamine (TEA). The neutralization was carried out in a 50/50 v/v of ethanol and 2 M aqueous solution of TEA at room temperature for 24 h. Afterward, the membrane was washed with water and then dried for 48 h under vacuum at 130 °C. The resulting [N117^{x-}(TEA$^+$)$_x$] membrane was swollen with TEA-TF ionic liquid at 80 °C for 48 h in a glovebox. The TEA-TF uptake was ∼30% and was evaluated with the following formula:

$$\%\text{TEA-TF} = [(w_f - w_i)/w_f)]*100$$

where w_f and w_i are the weight of the swollen and of the starting neutralized membrane, respectively.

2.3. Water Uptake (W.U.) and Membrane Reference Conditions (RC). The water uptake, the number of moles of water per mole of sulfonic/sulfonate groups (λ), and the residual water

(6) Alberti, G.; Casciola, M.; Massinelli, L.; Bauer, B. *J. Membr. Sci.* **2001**, *185*, 73.
(7) Wainright, J. S.; Litt, M. H.; Savinell, R. F. In *Handbook of Fuel Cells - Fundamentals, Technology and Applications*; Vielstich, W., Lamm, A., Gasteiger, H. A., Eds.; Wiley: Chichester, 2003; Vol. 3, p 436.
(8) Fontanella, J. J.; Wintersgill, M. C.; Wainright, J. S.; Savinell, R. F.; Litt, M. *Electrochim. Acta* **1998**, *43*, 1289.
(9) Martinelli, A.; Matic, A.; Jacobsson, P.; Börjesson, L.; Navarra, M. A.; Panero, S.; Scrosati, B. *J. Electrochem. Soc.* **2007**, *154*, G183.
(10) Ohno, H. *Electrochemical Aspects of Ionic Liquids*; John Wiley and Sons: Hoboken, NJ, 2005.
(11) Rogers, R. D.; Seddon, K. R. *Ionic liquids: Industrial applications for Green Chemistry*; American Chemical Society: Washington, DC, 2002.
(12) Belieres, J. P.; Angell, C. A. *J. Phys. Chem. B* **2007**, *111*, 4926.
(13) Ye, H.; Huang, J.; Xu, J. J.; Khalfan, A.; Greenbaum, S. G. *J. Electrochem. Soc.* **2007**, *154*, A1048.
(14) Doyle, M.; Choi, S. K.; Prolux, G. *J. Electrochem. Soc.* **2000**, *147*, 34.
(15) Fuller, J.; Carlin, R. *Molten Salts XII: Proceedings of the International Symposium*; The Electrochemical Society: Pennington, NJ, 1999; Vol. 27, p 99.
(16) Schmidt, C.; Glück, T.; Schmidt-Naake, G. *Chem. Eng. Technol.* **2008**, *31*, 13.
(17) Iojoiu, C.; Judeinstein, P.; Sanchez, J. Y. *Electrochim. Acta* **2007**, *53*, 1395.
(18) Judeinstein, P.; Iojoiu, C.; Sanchez, J. Y.; Ancian, B. *J. Phys. Chem. B* **2008**, *112*, 3680.

per sulfonate group of the membranes (λ_{RC}) were determined by measuring the TG profiles of the isothermal mass elimination vs time as reported elsewhere[19−21] and summarized in the available Supporting Information.

3. Results and Discussion

3.1. Water Uptake (W.U.), Morphology, and Thermal Analyses. The dependence of λ on t at 35 °C showed that the amount and rate of water absorption in the membranes increase in the order $[N117^{x-}(TEA^+)_x] < [N117^{x-}(TEA^+)_x/(TEA\text{-}TF)_y] <$ N117. The W.U. values of materials, which were measured at $t = \infty$, were 26.2, 11.4, 6.8 (wt%) respectively for N117, $[N117^{x-}(TEA^+)_x/(TEA\text{-}TF)_y]$, and $[N117^{x-}(TEA^+)_x]$. Therefore, neutralized Nafion is the most hydrophobic material. This evidence is easily explained if we consider the following: (a) the water uptake of these systems is mainly associated with the solvation of anion groups; (b) in $[N117^{x-}(TEA^+)_x]$ the perfluorosulfonate anion that interacts directly with the apical proton of the pyramidal TEA^+ cation is preserved from water solvation by the ethyl groups of the TEA^+ cation; (c) in $[N117^{x-}(TEA^+)_x/(TEA\text{-}TF)_y]$ the cation exchange processes, occurring in bulk materials between the sulfonate groups of neutralized Nafion and the TEA-TF domains embedded in the bulk, act to increase the disorder in the neighborhood of the ionomer anions, thus facilitating the H_2O solvation of these later; and (d) in $[N117^{x-}(TEA^+)_x/(TEA\text{-}TF)_y]$, the overall anion concentration, which is roughly 2/3 higher than that of $[N117^{x-}(TEA^+)_x]$, consists of the anionic species provided by the PCIL. It should be emphasized that the TF anion is expected to be solvated by water more easily than the neutralized Nafion host polymer. The morphology of $[N117^{x-}(TEA^+)_x]$ and $[N117^{x-}(TEA^+)_x/(TEA\text{-}TF)_y]$ membranes was analyzed by SEM in secondary electron measurements, revealing that the investigated materials consist of homogenous gummy glassy systems with very smooth surfaces. SEM X-ray fluorescence analyses with energy dispersive spectroscopy (XRD-EDS) carried out on different areas of membrane surfaces confirmed that C, O, F, and S are uniformly distributed over the entire material. Figure 1 shows the TG profiles of $[N117^{x-}(TEA^+)_x]$, $[N117^{x-}(TEA^+)_x/(TEA\text{-}TF)_y]$, N117, and pristine TEA-TF.

The inspection of the derivative curves of TG profiles shown in the insets of Figure 1 indicates that the first mass elimination occurring at $T < 150$ °C is associated with traces of water embedded in materials. The residual trace of water eliminated at $T < 150$ °C decreases in the order N117 > $[N117^{x-}(TEA^+)_x/(TEA\text{-}TF)_y]$ > TEA-TF > $[N117^{x-}(TEA^+)_x]$ with amounts of respectively 2.8 > 1.7 > 1.3 > 0.8 wt %. Actually, the water affinity seems to be in accordance with the W.U. behavior. The traces of water determined in the pristine PCIL are justified on the basis of the TEA-TF nanostructure, which probably acts to reduce the strength of the water−TF anion interactions and consequently its water adsorption. In accordance with other studies,[19−24] the second mass elimination of the N117 TG profile

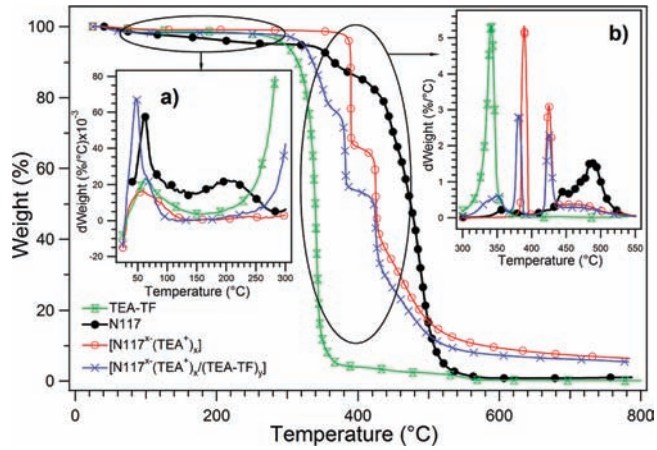

Figure 1. Thermograms (TGs) of $[N117^{x-}(TEA^+)_x]$, $[N117^{x-}(TEA^+)_x/(TEA\text{-}TF)_y]$, and reference materials. The insets show the derivative of TG profiles in the regions 30−300 °C (a) and 300−550 °C (b).

measured in the 170−250 °C temperature range corresponds to the decomposition of $-SO_3H$ groups (see inset (a) of Figure 1). This event is absent in the TG curves of $[N117^{x-}(TEA^+)_x]$ and $[N117^{x-}(TEA^+)_x/(TEA\text{-}TF)_y]$, thus indicating that in these samples the membranes are thermally stable respectively up to ca. 380 and 310 °C.[23,25] The weight losses occurring in the third region at $T > 300$ °C correspond to the decomposition of PCIL, Nafion backbone, and polyether side groups.[19−24] The TG profiles and the derivative curves (see insets (a) and (b) of Figure 1) indicate that pure PCIL starts to degrade at ca. 220 °C and that the membrane with the lowest thermal stability is $[N117^{x-}(TEA^+)_x/(TEA\text{-}TF)_y]$, which decomposes at ca. 310 °C. Results allow us to summarize that the thermal stability (a) increases for PCIL when it is incorporated in bulk $[N117^{x-}(TEA^+)_x]$ and (b) decreases for $[N117^{x-}(TEA^+)_x]$ when it is plasticized with the PCIL component. Although TG analyses were carried out in nitrogen and not in air, results allow us to infer that $[N117^{x-}(TEA^+)_x/(TEA\text{-}TF)_y]$ membranes present a high enough thermal stability to be implemented in high-temperature PEMFCs. The DSC profiles of the investigated materials are shown in Figure 2.

The analysis of the DSC profile of TEA-TF reveals the presence of two thermal transitions at 32 and −43.5 °C which, in accordance with other studies,[10,26] were attributed respectively to the first (T_{m1}) and second (T_{m2}) melting temperature of the water-TEA-TF and the pure PCIL domains, respectively. A further exothermal transition is revealed at −72.5 °C, which was assigned to the crystallization temperature (T_C).[26] The DSC profile of N117 in the temperature range 90−300 °C shows three thermal events, indicated as I, II, and III, peaking at ca. 150, 193, and 230 °C, respectively (Figure 2). In accordance with other studies,[23] I is assigned to the melting of small and imperfect fluorocarbon nanocrystalline domains of Nafion, II is attributed to the endothermic decomposition of acid $-SO_3H$ groups, and III corresponds to the melting of hydrophobic fluorocarbon microcrystalline regions in the Nafion membranes.[19−24] The DSC curves of materials indicate that (a) I and III peaks are measured for $[N117^{x-}(TEA^+)_x]$ and (b) only I is detected for the $[N117^{x-}(TEA^+)_x/(TEA\text{-}TF)_y]$ system. The absence of peak II in $[N117^{x-}(TEA^+)_x]$ and $[N117^{x-}(TEA^+)_x/(TEA\text{-}TF)_y]$

(19) Di Noto, V.; Gliubizzi, R.; Negro, E.; Vittadello, M.; Pace, G. *Electrochim. Acta* **2007**, *53*, 1618.
(20) Vittadello, M.; Negro, E.; Lavina, S.; Pace, G.; Safari, A.; Di Noto, V. *J. Phys. Chem. B* **2008**, *112*, 16590.
(21) Di Noto, V.; Piga, M.; Piga, L.; Polizzi, S.; Negro, E. *J. Power Sources* **2008**, *178*, 561.
(22) Di Noto, V.; Gliubizzi, R.; Negro, E.; Pace, G. *J. Phys. Chem. B* **2006**, *110*, 24972.
(23) Di Noto, V.; Piga, M.; Lavina, S.; Negro, E.; Yoshida, K.; Ito, R.; Furukawa, T. *Electrochim. Acta* **2009**, in press (doi:10.1016/j.electacta.2009.06.011).
(24) Di Noto, V.; Vittadello, M. *Electrochim. Acta* **2005**, *50*, 3998.
(25) De Almeida, S. H.; Kawano, Y. *J. Therm. Anal. Calorim.* **1999**, *58*, 569.
(26) Imai, Y.; Abe, H.; Goto, T.; Yoshimura, Y.; Kushiyama, S.; Matsumoto, H. *J. Phys. Chem. B* **2008**, *112*, 9841.

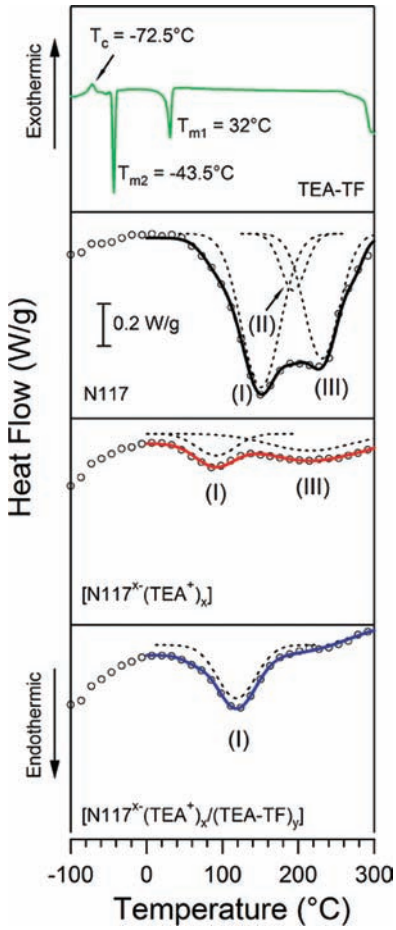

Figure 2. MDSC measurements of [N117^{x-}(TEA$^+$)$_x$], [N117^{x-}(TEA$^+$)$_x$/(TEA-TF)$_y$], and reference materials. Dashed lines show the peak decomposition by Gaussian functions. I, II, and III single out the endothermic peaks of the materials.

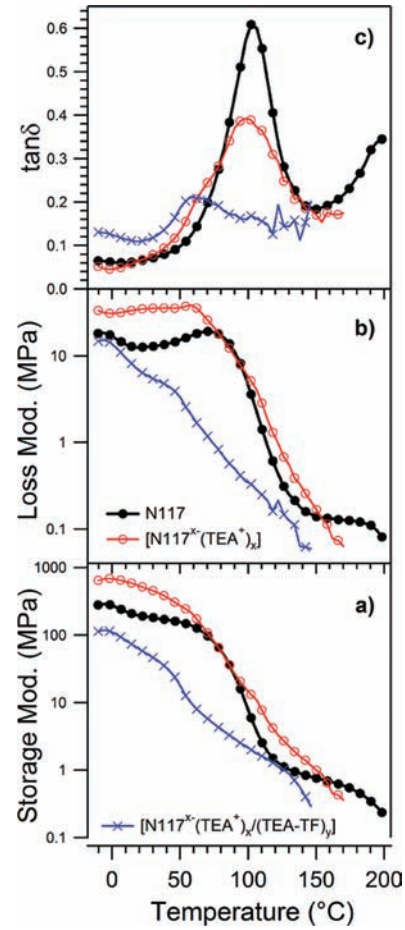

Figure 3. Storage modulus (E') (a), loss modulus (E'') (b), and tan δ (c) profiles vs temperature of materials. Measurements collected at 1 Hz with an amplitude of 4 μm.

membranes is in accordance with the derivative curves of TG profiles shown in the inset (a) of Figure 1, which reveals that the decomposition of $-SO_3^-$ groups occurs at temperatures higher than 300 °C. Furthermore, the thermal transition III, which is observed in N117 and [N117^{x-}(TEA$^+$)$_x$] with ΔH_{III} values respectively of 103.35 and 31.50 J/g, indicates the following: (a) in [N117^{x-}(TEA$^+$)$_x$] the neutralization of $-SO_3H$ with TEA$^+$ reduces the microcrystallinity of hydrophobic fluorocarbon domains to 30.5%; (b) in [N117^{x-}(TEA$^+$)$_x$/(TEA-TF)$_y$], owing to the plasticizing effect of incorporated TEA-TF, the residual microcrystallinity of the hydrophobic fluorocarbon regions present in [N117^{x-}(TEA$^+$)$_x$] is only slightly observed. Thermal event I peaks at temperatures decreasing in the order 150, 118, and 92 °C respectively for N117, [N117^{x-}(TEA$^+$)$_x$/(TEA-TF)$_y$], and [N117^{x-}(TEA$^+$)$_x$], thus proving that the size of the hydrophobic fluorocarbon nanodomains of neutralized Nafion is modulated concurrently. Indeed, it is expected that the sizes of PTFE-like nanodomains are (a) larger in N117; (b) of medium size in [N117^{x-}(TEA$^+$)$_x$/(TEA-TF)$_y$], due to the plasticizing effect of TEA-TF; and (c) of small size in [N117^{x-}(TEA$^+$)$_x$], owing to the presence of van der Waals interactions between ethyl-terminated side groups which are originated when $-SO_3^-$ anions are directly interacting with the apical proton of the pyramidal TEA$^+$ cation. These results are further supported by the perfect linearity of ΔH_I vs W.U. which demonstrates that as the ΔH_I value decreases, the hydrophobic character of side groups of samples increases, thus reducing the W.U. ability of materials. Taken together, results suggest the following: (a) the neutralization of N117 by TEA increases both the thermal stability and the hydrophobic character of side groups, thus reducing significantly the size of the hydrophobic nanoclusters of materials; (b) the doping of neutralized N117 with TEA-TF increases the sizes of the hydrophobic nanoclusters owing to the plasticization effect of TEA-TF; as a consequence, the dynamics of fluorocarbon backbone chains of [N117^{x-}(TEA$^+$)$_x$] are facilitated, giving rise to an increase of the size of close-packed fluorocarbon domains.

3.2. Dynamic Mechanical Studies. The temperature spectra of the storage (E') and loss (E'') modulus and tan δ of materials shown respectively in Figure 3a, b, and c were measured by using a dynamic oscillatory method with sinusoidal mechanical elongations of 4 μm at 1 Hz.

It should be observed that an irreversible elongation of samples occurred at temperatures above 170, 160, and 150 °C respectively for N117, [N117^{x-}(TEA$^+$)$_x$], and [N117^{x-}(TEA$^+$)$_x$/(TEA-TF)$_y$]. The analysis of E′, E″, and tan δ (Figure 3) shows that N117 at ca. 100 °C exhibits its typical α-relaxation event which, in accordance with other studies,[22,27] was attributed to the long-range motions of fluorocarbon backbone and side chains, which occur when in dipolar aggregates a weakening of electrostatic interactions takes place. It should be observed

(27) Page, K. A.; Cable, K. M.; Moore, R. B. *Macromolecules* **2005**, *38*, 6472.

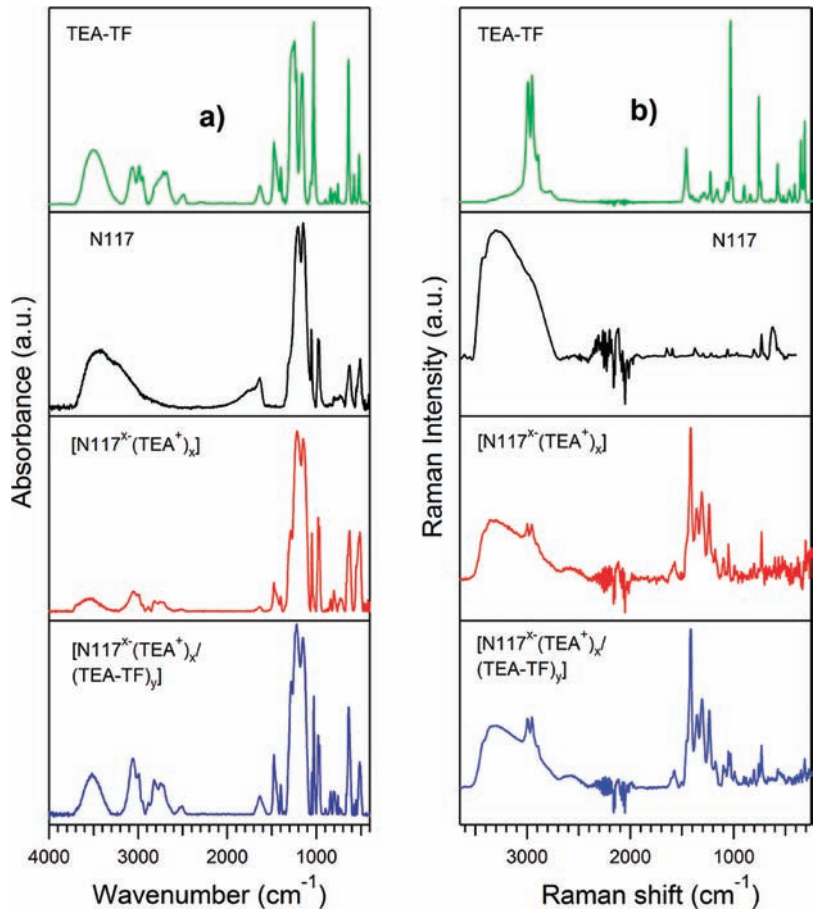

Figure 4. FT-IR ATR (a) and micro-Raman (b) spectra of [N117^{x-}(TEA^{+})$_x$], [N117^{x-}(TEA^{+})$_x$/(TEA-TF)$_y$], and reference materials. Micro-Raman measurements were obtained at an excitation wavelength of 514.5 nm.

that the intensity and the temperature of the maximum of the α relaxation peak T_α decreases in the order N117 > [N117^{x-}(TEA^{+})$_x$] > [N117^{x-}(TEA^{+})$_x$/(TEA-TF)$_y$], showing values equal to 103, 98, and 58 °C, respectively. Results reveal that the loss of energy corresponding to the motion of backbone and side chains in cluster aggregates (a) is higher in N117, where hydrogen bonding networks characterized by strong dipole−dipole interactions are expected; (b) is reduced in [N117^{x-}(TEA^{+})$_x$] where, as shown by the above-described DSC studies, weak van der Waals interactions are observed between ethyl-terminated side groups, but with more hindered steric interferences; and (c) is very low in [N117^{x-}(TEA^{+})$_x$/(TEA-TF)$_y$], where the sterically hindered neutralized side groups are solvated and plasticized by TEA-TF. The values of the storage modulus at 6 °C resulted in 650, 241, and 94 MPa respectively for [N117^{x-}(TEA^{+})$_x$], N117, and [N117^{x-}(TEA^{+})$_x$/(TEA-TF)$_y$]. The dependence of E' and T_α on ΔH_I indicates that, with respect to N117, a strong improvement of E' value is obtained in [N117^{x-}(TEA^{+})$_x$] owing to the presence in the bulk material of strong steric hindrance effects between neutralized side groups. In addition, in this latter sample the value of T_α, which is slightly lower than that of N117 reference, is in agreement with DSC results (peak I) and is correlated to the decrease of the size of the fluorocarbon hydrophobic nanodomains of neutralized Nafion and to their concurrent mobility. The reciprocal mobility of hydrophobic nanodomains is modulated by the strength of the interactions and by the hindering ability of side groups. In [N117^{x-}(TEA^{+})$_x$/(TEA-TF)$_y$] the incorporated TEA-TF, owing to its plasticization effect, modifies significantly the mechanical properties of neutralized N117 by reducing both the steric hindrance and the strength of the dipole−dipole interactions taking place between the side groups.

3.3. Vibrational Spectroscopy Studies. Vibrational studies were carried out to gain information on the secondary structure of the Nafion host polymer in the materials and to understand the interactions taking place in the bulk between the macromolecular system and TEA-TF. Figure 4a and b show the FT-IR ATR and the FT-Raman spectra of [N117^{x-}(TEA^{+})$_x$] and [N117^{x-}(TEA^{+})$_x$/(TEA-TF)$_y$]. For the sake of clarity, Nafion and TEA-TF reference spectra measured under the same conditions are also included.

The analysis of the spectral profiles of Figure 4a and b allows us to disclose that [N117^{x-}(TEA^{+})$_x$] and [N117^{x-}(TEA^{+})$_x$/(TEA-TF)$_y$] present the typical spectral features characterizing the Nafion component[19−21,23] and the TEA-TF PCIL.[28−31] In particular, it is possible to observe peaks associated with the following: (a) CF regions in the ranges 1377−1130 and 792−509 cm^{-1}, attributed to the fluorocarbon chain modes of PTFE-like domains of Nafion; (b) polyether side chain modes in the region 993−957 cm^{-1}; (c) the terminal sulfonate anion

(28) Lin-Vein, D.; Colthup, N. B.; Fateley, W. G.; Grasselli, J. G. *The Handbook of Infrared and Raman Characteristic Frequencies of Organic Molecules*; Academic Press: Boston, 1991.
(29) Fernandez, L. E.; BenAltabef, A.; Varetti, E. L. *Spectrochim. Acta A* **1996**, *52*, 287.
(30) Alia, J. M.; Edwards, H. G. M. *Vib. Spectrosc.* **2000**, *24*, 185.
(31) Alia, J. M.; Edwards, H. G. M.; Navarro, F. J. G.; Lawson, E. E. *J. Mol. Struct.* **2001**, *565*, 43.

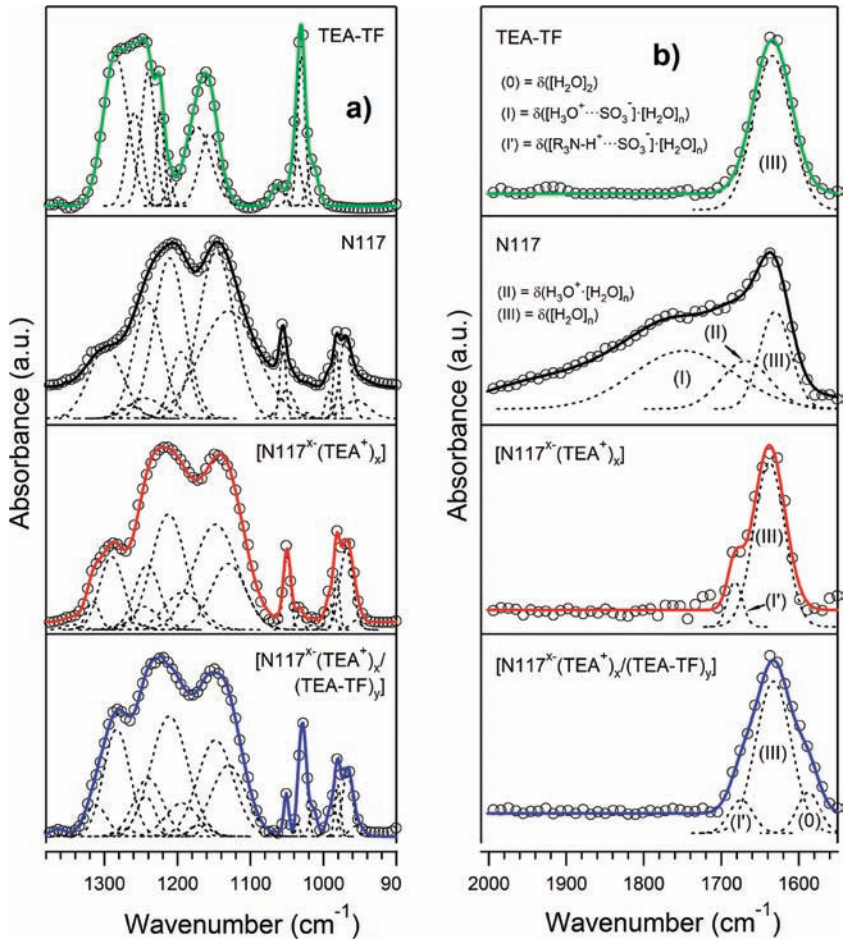

Figure 5. Decomposition by Gaussian functions of the FT-IR ATR spectral ranges corresponding to CF (a) and water bending (b) regions.

vibrations of Nafion; (d) the triflate anion vibrational modes, $CF_3SO_3^-$; (e) the tertiary ethyl amine cation vibrations, Et_3N-H^+; and (f) the vibrational modes of water species embedded in bulk membranes. The frequencies of the vibrational peaks measured in FT-IR ATR and FT-Raman spectra were assigned correlatively on the basis of other studies[19−21,23,28−31] (see Table S1 shown in the Supporting Information). The detailed analysis of the CF region of the FT-IR ATR profiles shown in Figure 5a was carried out as outlined in previous studies.[19−21,23,32]

The results, which are in accordance with other investigations,[19−21,23] permitted us to affirm that the intensities peaking at 1132, 1196, 1245, and 1266 cm^{-1} are associated to the 10_3 helical conformation of the fluorocarbon chains of the PTFE-like nanodomains of Nafion, while the bands at 1148, 1212, 1241, and 1299 cm^{-1} are attributed to fluorocarbon chains with a 15_7 helical conformation. Therefore, in $[N117^{x-}(TEA^+)_x]$ and $[N117^{x-}(TEA^+)_x/(TEA\text{-}TF)_y]$ the hydrophobic PTFE domains of the Nafion host polymer are based on a mixture of polymer chain backbones with 15_7 and 10_3 helical conformation geometries. The relative concentration of each type of helical conformation was determined on the basis of the method outlined elsewhere[23] by using the band areas of the CF_2 antisymmetric stretching vibrations of the A_2 species of both 10_3 and 15_7 helical conformations, respectively, at 1245 and 1212 cm^{-1} and the equation $\rho = A_{1245}/(A_{1245} + A_{1212})$. Band areas were evaluated by decomposition with Gaussian functions[32] of the CF region of studied materials (Figure 5a). Owing to strong spectral interferences with the peaks of TEA-TF, it was not possible to determine a reliable ρ value for the $[N117^{x-}(TEA^+)_x/(TEA\text{-}TF)_y]$ material. ρ, which is the approximate fraction of fluorocarbon chains with 10_3 helical conformation geometries, was 0.122 and 0.118 for $[N117^{x-}(TEA^+)_x]$ and the N117 reference, respectively. These values are in accordance with other studies on pristine Nafion,[19−21,23] and no modulation of the conformational composition in fluorocarbon hydrophobic domains occurs when N117 is neutralized by triethylamine. It should be noted that this evidence is in contrast with other studies.[19−21,23] Indeed, the latter report that the M_xO_y-Nafion interactions, where M_xO_y is a transition metal oxide, modulate significantly the concentration of 10_3 and 15_7 helical conformations in hybrid inorganic−organic [Nafion/$(M_xO_y)_n$] membranes. In addition, the comparison in the CF region of $[N117^{x-}(TEA^+)_x]$ and $[N117^{x-}(TEA^+)_x/(TEA\text{-}TF)_y]$ Raman spectra indicates that no significant change in the shape of the peaks diagnostic of fluorocarbon chain conformations is detected, thus allowing us to affirm that the structure and the composition of hydrophobic domains of the materials proposed in this work are similar to those of pristine N117. This evidence is in agreement with the studies of Martinelli et al.,[9] which reported that the interactions between $TFSI^-$ ionic liquids and a PVDF matrix are absent or negligible.

Further insights into the strength of the interactions between the PCIL and the polymer matrix of neutralized N117 were

(32) Di Noto, V. *J. Phys. Chem. B* **2000**, *104*, 10116.

sought by carrying out a detailed analysis on the peaks of the triflate anion vibrational modes, which are diagnostic of ion association phenomena of triflate salts in several solutions.[9,30−33] In particular, the triflate Raman peaks at ca. 760 and 1034 cm^{-1} were analyzed. The band at ca. 760 cm^{-1} is attributed to the $\nu_3(A_1)$ mode corresponding to the symmetric bending mode of the $-CF_3$ triflate anion. As reported elsewhere,[29−31] the $\nu_3(A_1)$ vibration can be split into three components peaking at 755, 758, and 762 cm^{-1}, which were associated with free anions, ion pairs, and higher ion aggregates, respectively. The mode at ca. 760 cm^{-1} is observed in both TEA-TF and $[N117^{x-}(TEA^+)_x/(TEA\text{-}TF)_y]$, thus suggesting that the confinement of TEA-TF in the neutralized N117 matrix does not alter the state of the pristine PCIL which corresponds to that of higher ion aggregates. The band at 1034 cm^{-1} is assigned to the $\nu_2(A_1)$ mode of the symmetric S−O stretching of the triflate anion. It was reported that the $\nu_2(A_1)$ mode can be detected in the material at 1034, 1042, and 1052 cm^{-1} when triflate is present as a free anion, ionic pairs, and higher aggregates, respectively.[31] On the basis of the $\nu_2(A_1)$ mode it should be concluded that triflate is present as a free anion. This result at first seems to be in contradiction with the conclusion achieved by the $\nu_3(A_1)$ mode. Actually, both indications drawn by $\nu_2(A_1)$ and $\nu_3(A_1)$ modes are true and in accordance with other recent studies,[26] thus suggesting that the PCIL domains consist of higher triflate aggregates organized into anionic micelle-like nanoparticles having (a) the hydrophobic CF_3-tails in the bulk "core" of the micelle (thus, triflate molecules can efficiently interact with each other by van der Waals forces through CF_3-groups) and (b) the hydrophilic sulfonate anion groups located on the outer surface of the micelle-like nanoparticle (thus, the latter behaves like a "free" macroanion group). Results point out that (a) the nanomorphology of $[N117^{x-}(TEA^+)_x]$ provides a porous environment adequate to preserve the *micelle-like nanostructure of triflate aggregations* (MTAs) typical of pristine TEA-TF and (b) the interactions MTAs•••••MTAs and MTAs•••••Nafion take place through the formation and breaking of TEA^+ cation bridges between sulfonate groups present on the surface of MTAs and fixed in Nafion side groups.

The different species and interactions characterizing the traces of water adsorbed in $[N117^{x-}(TEA^+)_x]$ and $[N117^{x-}(TEA^+)_x/(TEA\text{-}TF)_y]$ membranes were studied by decomposing the water bending region 1590−1770 cm^{-1} by Gaussian functions (Figure 5b) as described elsewhere.[32,34] Five overlapped bands indicated as 0, I, I′, II, and III were detected. Peak 0 was assigned to the bending mode of water species in the dimer form, $\delta([H_2O]_2)$.[19,20] The presence of this spectral feature in $[N117^{x-}(TEA^+)_x/(TEA\text{-}TF)_y]$ suggests that water aggregates are located in the bulk environments where the dielectric constant is low. Peak III was attributed to the bending mode of bulk water, $\delta([H_2O]_n)$.[19,20,35] Bending vibration II was ascribed to water molecules solvating oxonium ions, $\delta(H_3O^+\cdot[H_2O]_n)$.[19,20,35] I corresponds to the bending vibration of water molecules solvating the oxonium−R−SO_3^- ion pair, $\delta(H_3O^+\cdots SO_3^-]\cdot[H_2O]_n)$.[19,20,35] I′ is the bending mode of water molecules solvating the ionic couple triethylammonium-sulfonate group, $\delta[R_3N{-}H^+\cdots SO_3^-]\cdot[H_2O]_n$. In addition, the 2500−4000 cm^{-1} region allowed us to reveal the presence of five broad peaks associated with the stretching vibrations of "free" and hydrogen bonded hydroxyls of water.[20,35] In particular, the following broad peaks assigned to water stretching modes were detected: (a) the IV antisymmetric and the III symmetric stretching vibrations, ν(O−H), respectively in the 3430−3573 and 3576−3623 cm^{-1} range, of water molecules not involved in hydrogen bonding structures; (b) the II, $\nu([H_2O]_n)_{hy}$, in the range 3247−3455 cm^{-1} of hydrogen-bonded bulk water domains; (c) the I, $\nu_{as}(H_3O^+\cdots SO_3^-]\cdots[H_2O]_n)$, at ca. 2920 cm^{-1} of antisymmetric OH stretching vibrations of hydroxonium ions; and (d) the I′, $\nu(N{-}H^+\cdot[H_2O]_n)_{hy}$, in the range 3065−3049 cm^{-1} of OH stretching vibrations of water interacting with triethylammonium ions.

Table 1 reports semiquantitative information on (a) the concentration of each different type of water species, f_i, present in bulk materials and (b) the fractions of both "free" water and water involved in hydrogen bonding networks, h_i, in bulk materials. The peak parameters reported in Table 1 were obtained by Gaussian spectral decomposition of MIR spectra (Figure 5b). f_i and h_i values were determined using the peak parameters as described elsewhere.[19−21,23,34] The spectral features of the water component and the values of f_i and h_i (Table 1) allow us to conclude that, with respect to pristine N117, the dipolar domains of the proposed membranes are highly hydrophobic. Indeed, the traces of water are embedded as bulk water nanoparticles for ca. 88% and 76% for $[N117^{x-}(TEA^+)_x]$ and $[N117^{x-}(TEA^+)_x/(TEA\text{-}TF)_y]$, respectively. In addition, the amounts of water solvating the $R_3N{-}H^+\cdots{}^-SO_3-$ bridges (Table 1) of $[N117^{x-}(TEA^+)_x]$ and $[N117^{x-}(TEA^+)_x/(TEA\text{-}TF)_y]$ are similar, with values on the order of ca. 12 and 11%, respectively. This result and the unitary value of the fraction of bulk water in TEA-TF demonstrate that, in the proposed membranes, water, which is not associated in bulk nanodrops, preferentially solvates the $R_3N{-}H^+\cdots{}^-SO_3-$ bridges of the sulfonate side groups of Nafion. Furthermore, the presence of ca. 13% of water in dimer form and the slightly lower amount of bulk water nanoparticles (76%) reveals that in $[N117^{x-}(TEA^+)_x/(TEA\text{-}TF)_y]$ the adsorbed TEA-TF acts to reduce the differences in dielectric constant existing between the dipolar and the hydrophobic domains of the pristine $[N117^{x-}(TEA^+)_x]$ material. This leads to the reduction of the clustering process of water nanodrops and to the promotion of the formation of water dimers, which are the water aggregates with the lowest possible dipolar moment. Taken together, vibrational studies allowed us to determine the following: (a) the neutralization of N117 with TEA to prepare $[N117^{x-}(TEA^+)_x]$ and its subsequent treatment with TEA-TF to obtain $[N117^{x-}(TEA^+)_x/(TEA\text{-}TF)_y]$ do not change the conformational composition of hydrophobic fluorocarbon domains of the pristine N117 matrix; (b) the confinement of TEA-TF in the $[N117^{x-}(TEA^+)_x]$ matrix does not alter significantly the structural scenario which characterizes the domains of pristine TEA-TF; (c) the dipolar domains of $[N117^{x-}(TEA^+)_x]$ and $[N117^{x-}(TEA^+)_x/(TEA\text{-}TF)_y]$ are more hydrophobic than that of pristine acid N117; (d) the triflate anion in dipolar domains of $[N117^{x-}(TEA^+)_x/(TEA\text{-}TF)_y]$ forms micelle-like nanoaggregates which consist of a "core" of CF_3-groups having the sulfonate polar heads on the outer surface of the nanocluster; (e) in $[N117^{x-}(TEA^+)_x]$ and $[N117^{x-}(TEA^+)_x/(TEA\text{-}TF)_y]$ water is present for the most part as bulk water nanoaggregates; the remaining amount solvates preferentially the $R_3N{-}H^+\cdots{}^-SO_3-$ bridges of sulfonate side groups of Nafion.

(33) Rey, I.; Johansson, P.; Lindgren, J.; Lassegues, J. C.; Grondin, J.; Servant, L. *J. Phys. Chem. A* **1998**, *102*, 3249.
(34) Di Noto, V.; Longo, D.; Münchow, V. *J. Phys. Chem. B* **1999**, *103*, 2636.
(35) Hofmann, D. W. M.; Kuleshova, L.; D'Aguanno, B.; Di Noto, V.; Negro, E.; Conti, F.; Vittadello, M. *J. Phys. Chem. B* **2009**, *113*, 632.

Table 1. Band Parameters of the FT-IR ATR Water Bending and Stretching Modes for TEA-TF, N117, [$N117^{x-}(TEA^{+})_x$], and [$N117^{x-}(TEA^{+})_x$/$(TEA\text{-}TF)_y$]

material	band	frequency/cm^{-1}	A_i[a]	$fwhm_i$	f_i[b]	h_i[b]
TEA-TF	$\delta([H_2O]_n)$ (III)	1634	3.24 ± 0.01	57.4 ± 0.3	1	
	$\nu(N-H^{+}\cdot[H_2O]_n)_{hy}$ (I′)	3065	10.73 ± 0.05	90.0 ± 0.5		0.20
	$\nu([H_2O]_n)_{hy}$ (II)	3394	13.6 ± 0.1	180 ± 0.2		0.25
	ν_s(O−H) (III)	3519	27.9 ± 0.1	182 ± 1		0.52
	ν_{as}(O−H) (IV)	3595	1.97 ± 0.06	74 ± 2		0.04
N117	$\delta[H_3O^{+}\cdots SO_3^{-}]\cdot[H_2O]_n)$ (I)	1751	0.93 ± 0.1	156 ± 12	0.52	
	$\delta(H_3O^{+}\cdot[H_2O]_n)$ (II)	1670	0.38 ± 0.2	76 ± 17	0.21	
	$\delta([H_2O]_n)$ (III)	1631	0.47 ± 0.1	48 ± 2	0.26	
	$\nu_{as}([H_3O^{+}\cdots SO_3^{-}]\cdots[H_2O]_n)$ (I)	2920	2.39 ± 0.07	371 ± 10		0.08
	$\nu([H_2O]_n)_{hy}$ (II)	3247	14.90 ± 0.09	366 ± 3		0.52
	ν_s(O−H) (III)	3456	7.83 ± 0.07	213 ± 2		0.28
	ν_{as}(O−H) (IV)	3576	3.27 ± 0.04	143 ± 1		0.12
$[N117^{x-}(TEA^{+})_x]$	$\delta[R_3N-H^{+}\cdots SO_3^{-}]\cdot[H_2O]_n)$ (I′)	1682	0.018 ± 0.001	22.6 ± 1	0.12	
	$\delta([H_2O]_n)$ (III)	1638	0.134 ± 0.002	47.0 ± 0.6	0.88	
	$\nu(N-H^{+}\cdot[H_2O]_n)_{hy}$ (I′)	3049	1.03 ± 0.01	133 ± 1		0.47
	$\nu([H_2O]_n)_{hy}$ (II)	3455	0.37 ± 0.02	159 ± 3		0.17
	ν_s(O−H) (III)	3573	0.68 ± 0.01	154 ± 6		0.32
	ν_{as}(O−H) (IV)	3678	0.09 ± 0.02	64 ± 4		0.04
$[N117^{x-}(TEA^{+})_x/(TEA\text{-}TF)_y]$	$\delta[R_3N-H^{+}\cdots SO_3^{-}]\cdot[H_2O]_n)$ (I′)	1674	0.07 ± 0.001	36.38 ± 0.7	0.11	
	$\delta([H_2O]_n)$ (III)	1632	0.47 ± 0.01	54.03 ± 0.4	0.76	
	$\delta([H_2O]_2)$ (0)	1587	0.081 ± 0.002	34.8 ± 0.5	0.13	
	$\nu(N-H^{+}\cdot[H_2O]_n)_{hy}$ (I′)	3062	2.59 ± 0.01	97 ± 3		0.41
	$\nu([H_2O]_n)_{hy}$ (II)	3392	0.26 ± 0.05	98 ± 1		0.04
	ν_s(O−H) (III)	3516	3.31 ± 0.01	175 ± 2		0.53
	ν_{as}(O−H) (IV)	3623	0.14 ± 0.02	100 ± 5		0.02

[a] A_i and $fwhm_i$ are the band area and the full width at half-maximum of the peak centered at the frequency reported in the third column. [b] f_i is the fraction of water species present in bulk material. h_i is the fraction of water involved in hydrogen bonding networks. The semiquantitative values of f_i and h_i were determined by the formula $x_i = A_i/\Sigma$, where $x_i = f_i$ and h_i. A_i is the band area of peak i-th. $\Sigma = \sum_{i=1}^{n} A_i$, and n is the number of species considered.

3.4. Broad Band Dielectric Spectroscopy Studies. The conductivity mechanism in terms of charge migration processes and the dielectric relaxations of $[N117^{x-}(TEA^{+})_x]$, $[N117^{x-}(TEA^{+})_x/(TEA\text{-}TF)_y]$, and the reference materials was investigated by broad band dielectric spectroscopy (BDS) in frequency and temperature ranges of 10 mHz−10 MHz and −155−155 °C, respectively. The simultaneous 3D representation of the measured spectra of the real ($\varepsilon'(\omega)$) and the imaginary ($\varepsilon''(\omega)$) (Figure 6) components of permittivity was carefully studied.

It should be observed that, in correspondence of the transition events detected by both DSC and DMA analyses, the profiles of $\varepsilon'(\omega)$ and $\varepsilon''(\omega)$ abruptly changed. Four different dielectric regions delimited by the temperatures of the three DSC thermal events disclosed at 32, −43.5, and −75.2 °C and discussed above were detected. In detail, the temperature ranges $T > 32$, $32 > T > -43.5$, $-43.5 > T > -75.2$, and $T < -75.2$ °C were singled out as HT, MT, LT, and VLT, respectively. The qualitative study of the $\varepsilon'(\omega)$ and $\varepsilon''(\omega)$ curves at frequencies below 300 Hz and in the range between 1 kHz and 1 MHz allowed to disclose two distinct polarization phenomena in the HT region and one in the remaining low-temperature regions. It was reported that similar spectral features are commonly observed for ion-conducting polymer electrolytes composed of a two-phase dispersion consisting of spherical nanoparticles with a high dielectric constant embedded into a bulk matrix with a low dielectric constant.[36] The materials proposed here behave in accordance with these studies. It should be emphasized that, in agreement with other studies,[37−39] the morphology of N117 can be considered similar to that of the above-described nanocomposite mixture. Indeed, it is composed of PTFE-like hydrophobic fluorocarbon domains with a dielectric constant close to ca. 2.2 hosting hydrophilic polar domains with a high dielectric constant, close to that of water (ca. 80). On this basis, in accordance with other studies on pristine Nafion, the polarization event peaking at low frequencies in our materials was attributed to the interfacial polarization or the Maxwell−Wagner phenomenon.[40,41] This latter event occurs in heterogeneous systems when they are endowed with boundaries between phases characterized by a different dielectric constant.[40−42] Thus, the interfacial polarization is generated owing to the buildup of space charges near the interfaces between the various phases. The high-frequency polarization event was ascribed to the electrode polarization phenomenon which gives rise to conductive relaxations associated with ion accumulation processes near the electrodes rather than dielectric relaxations.[42,43] Further insights into the complex scenario of the dielectric relaxations resulting from 3D plots of permittivity components (Figure 6) were obtained by analyzing the temperature spectra of tan $\delta(\omega) = \varepsilon''(\omega)/\varepsilon'(\omega)$ at 20 Hz, 1 kHz, and 10 kHz (Figure 7).

It is to be emphasized that TEA-TF (Figure 7) (a) at $T > -43.5$ °C presents the expected solid-state T_g transition, which gives rise to the PCIL α_s-relaxation, and (b) at $T > 32$ °C α-

(36) Furukawa, T.; Yasuda, K.; Takahashi, Y. *IEEE Trans. Dielectr. Electr. Insul.* **2004**, *11*, 65.
(37) Rubatat, L.; Rollet, A. L.; Gebel, G.; Diat, O. *Macromolecules* **2002**, *35*, 4050.
(38) Schmidt-Rohr, K.; Chen, Q. *Nat. Mater.* **2008**, *7*, 75.
(39) Dura, J. A.; Murthi, V. S.; Hartman, M.; Satija, S. K.; Majkrzak, C. F. *Macromolecules* **2009**, *42*, 4769.
(40) Di Noto, V.; Negro, E.; Lavina, S. *Fuel Cell Membranes*; in press on ACS Symposium Series; American Chemical Society: Washington, DC, 2009.
(41) Di Noto, V.; Piga, M.; Pace, G.; Negro, E.; Lavina, S. *ECS Trans.* **2008**, *16*, 1183.
(42) Beek, L. K. H. In *Progress in dielectrics*; Birks, J. B., Ed.; Heywood: London, 1967; Vol. 7, p 69.
(43) Schönhals, A.; Kremer, F. In *Broadband Dielectric Spectroscopy*; Kremer, F., Schönhals, A., Eds.; Springer-Verlag: Berlin, 2003; p 59.

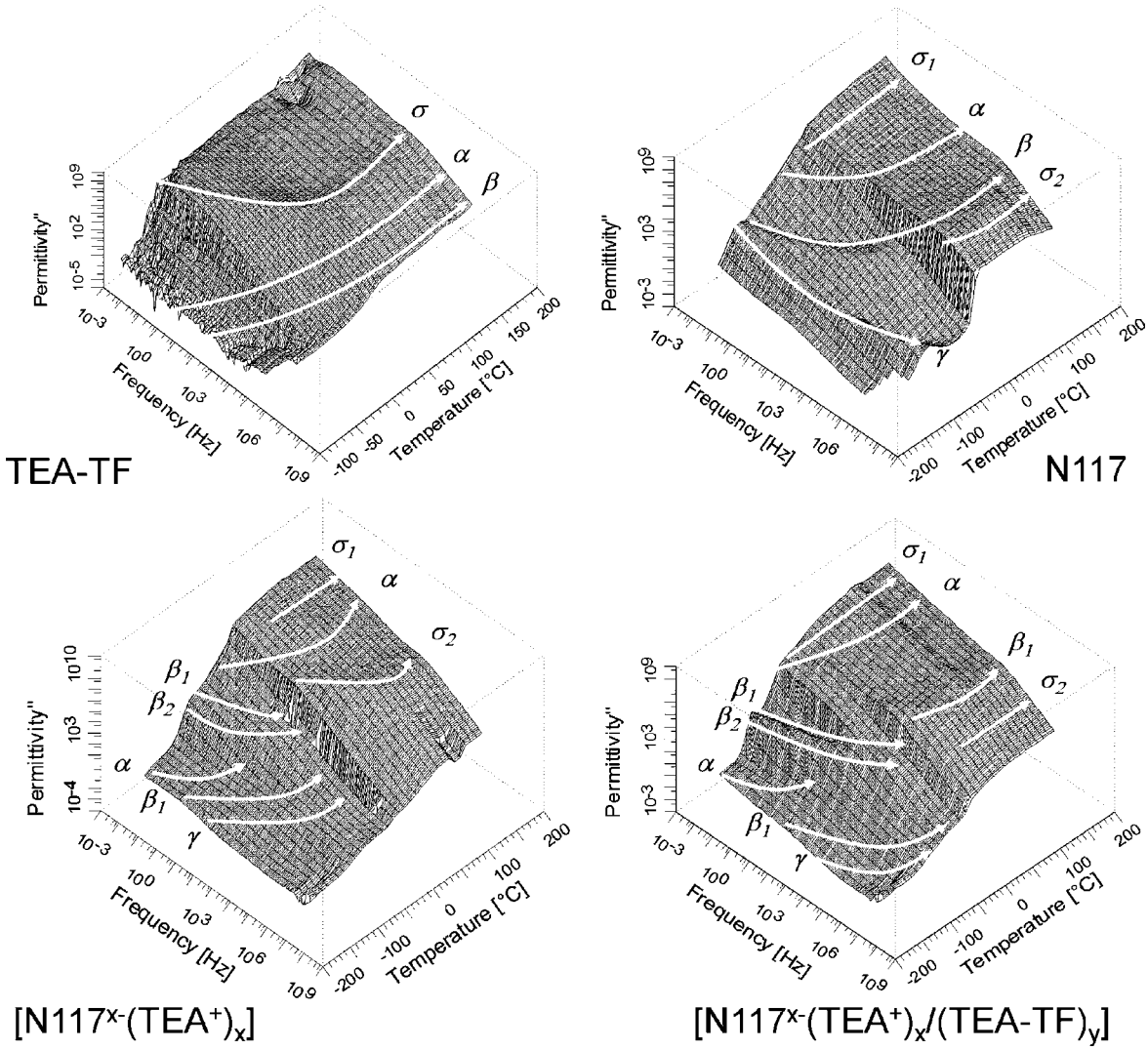

Figure 6. 3D plots of the imaginary component of the permittivity $\epsilon''(\omega)$ of materials.

and β-events typical of relaxation modes of liquid bulk PCIL are detected. In accordance with previous dynamic mechanical and dielectric studies,[42−44] N117 at $T < 0$ °C presents three relaxation peaks labeled α, β, and γ in descending order of temperature. The α mode was attributed to the glass transition of the fluorocarbon matrix. β corresponds to the relaxation of the ionic domains generated by the aggregation of polar acid side groups, and γ to the short-range molecular motions of the $-CF_2-$ backbone groups. Figures 6 and 7 show the prominent changes which happen in the dielectric spectra after the neutralization of N117. In particular, it is observed that four relaxation modes are observed in $[N117^{x-}(TEA^+)_x]$ and $[N117^{x-}(TEA^+)_x/(TEA\text{-}TF)_y]$ temperature spectra (Figure 7). These peaks, which were labeled in descending order of temperature as α, β_1, β_2, and γ, were attributed on the basis of other studies as follows:[42−45] (a) α to the glass transition of the fluorocarbon backbone matrix; (b) β_1 to the relaxation modes of ether side groups bonded to the $-CF_2-$ backbone; (c) β_2 to the relaxation mode of the ether side groups bonded to terminal $-SO_3^-$ functionalities; and (d) γ to the modes associated to local short-range motions of the $-CF_2-$ backbone.

A comparison of the temperature spectra shown in Figure 7 allows us to affirm that β_1 and β_2 are relaxation modes diagnostic of the interactions occurring in the hydrophilic domains of membranes. A quantitative study of the phenomena described above was carried out by analyzing the permittivity spectra using the generalized empirical equation:[40,41,46,47]

$$\varepsilon^*(\omega) = \varepsilon_\infty + \sum_{j=1}^{2} \frac{\sigma_{DC,j}(i\omega\tau_{el,j})^{\gamma_j}}{i\omega[1 + (i\omega\tau_{el,j})^{\gamma_j}]} + \sum_{k=1}^{n} \frac{\Delta\varepsilon_k}{[1 + (i\omega\tau_k)^{\alpha_k}]^{\beta_k}} \quad (1)$$

where $\sigma_{DC,1}$ and $\sigma_{DC,2}$ are the interfacial ($j = 1$) and sample ($j = 2$) dc conductivities, respectively. $\tau_{el,j}$ is the relaxation time associated with the j-th polarization phenomenon. γ_j are parameters describing the distribution of relaxation times. $\tau_k = (2\pi f_k)^{-1}$ is the dielectric relaxation time (f_k in Hz is the frequency of the peak maximum). $\Delta\varepsilon_k$ is the relaxation strength, and α_k and β_k are shape parameters describing the symmetric and asymmetric broadening of the k-th relaxation peak. The first

(44) Hodge, M. I.; Eisenberg, A. *Macromolecules* **1978**, *11*, 289.
(45) Kyu, T.; Hashiyama, M.; Eisenberg, A. *Can. J. Chem.* **1983**, *61*, 680.
(46) Di Noto, V.; Vittadello, M.; Greenbaum, S. G.; Suarez, S.; Kano, K.; Furukawa, T. *J. Phys. Chem. B* **2004**, *108*, 18832.
(47) Di Noto, V.; Lavina, S.; Negro, E.; Vittadello, M.; Conti, F.; Piga, M.; Pace, G. *J. Power Sources* **2009**, *187*, 57.

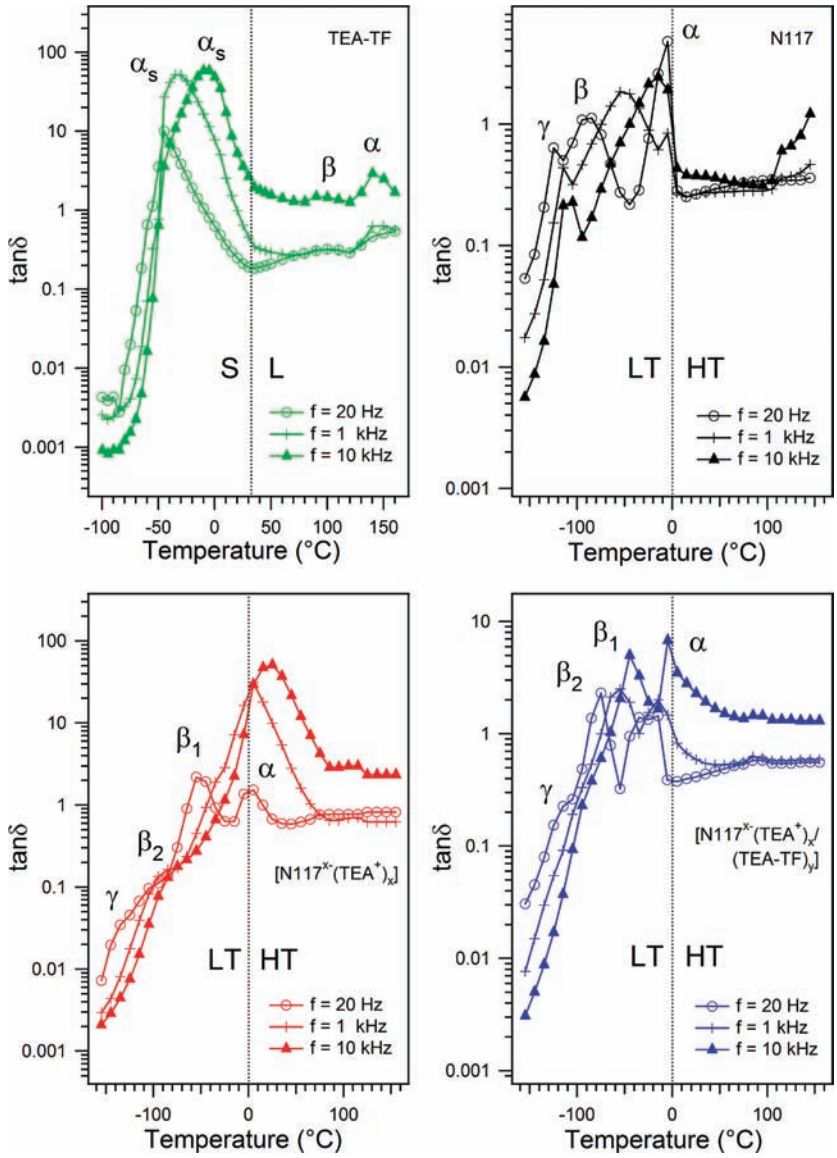

Figure 7. Temperature dependence of tanδ for the materials. S and L indicate the solid and liquid state of TEA-TF. LT and HT single out the temperature regions at $T > 0$ °C and T ≤ 0 °C, respectively.

and the third term of eq 1 simulate the dielectric relaxations of materials, while the second term accounts for the polarization events and the dc conductivity. The goodness of the fitting process was checked by comparing the $\sigma_{DC,1}$ and $\sigma_{DC,2}$ values determined with eq 1 respectively in the HT region and at $T <$ 5 °C with that of the bulk conductivity of the materials, σ_{DC}, measured as described elsewhere[48] at the plateaus of the σ' profiles. To reveal the correlations taking place between charge migration mechanisms and the relaxation phenomena of the bulk polymer, the parameters determined by fitting the complex permittivity spectra shown in Figure 6 with eq 1 were analyzed vs temperature and sample composition. For the sake of brevity, selected parameters are described in the following discussion. Figure 8 shows the dependence of $\sigma_{DC,1}$ and $\sigma_{DC,2}$ values on temperature.

It should be pointed out that the bulk conductivity (σ_{DC}) of materials (a) corresponds with $\sigma_{DC,2}$ ($\sigma_{DC} = \sigma_{DC,2}$) and $\sigma_{DC,1}$ ($\sigma_{DC} = \sigma_{DC,1}$) respectively at $T > 5$ and $T < 5$ °C and (b) presents a stability range of conductivity (SRC) enhanced up to 155 °C (N117 reference shows an SRC of $5 < T < 105$ °C). The comparison of the SRCs of the proposed materials shows that at 145 °C σ_{DC} decreases in the order [N117^{x-}(TEA$^+$)$_x$/(TEA-TF)$_y$] > N117 > [N117^{x-}(TEA$^+$)$_x$] with values of ca. $7.3 \times 10^{-3} > 6.1 \times 10^{-3} > 9.7 \times 10^{-4}$ S·cm^{-1}, respectively. At temperatures lower than 105 °C, the conductivity descends in the order N117 > [N117^{x-}(TEA$^+$)$_x$/(TEA-TF)$_y$] > [N117^{x-}(TEA$^+$)$_x$]. As expected, results confirmed that neutralized Nafion presents the lowest conductivity, while the presence of TEA-TF in [N117^{x-}(TEA$^+$)$_x$/(TEA-TF)$_y$] increases the conductivity of the membrane by at least 1 order of magnitude. At $T > 5$ °C the dependence of conductivity on temperature ($\sigma_{DC} = \sigma_{DC,2}$) follows the typical Vogel−Tamman−Fulcher (VTF) dependence,[22,48] thus demonstrating that the segmental motion of fluorocarbon chains are crucial in modulating the long-range charge migration of these materials. In addition, in all of the investigated temperature ranges, $\sigma_{DC,1}$ vs $1/T$ (a) presents values 4 orders of magnitudes lower that that of $\sigma_{DC,2}$, (b) exhibits values typical of low-conducting polymer electrolytes, and (c)

(48) Di Noto, V. *J. Phys. Chem. B* **2002**, *106*, 11139.

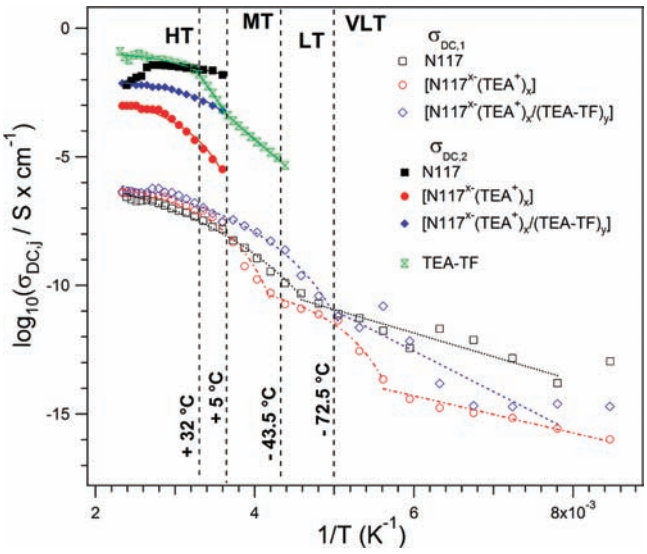

Figure 8. Temperature dependence of $\sigma_{DC,1}$ and $\sigma_{DC,2}$ of $[N117^{x-}(TEA^+)_x]$, $[N117^{x-}(TEA^+)_x/(TEA\text{-}TF)_y]$, and reference materials. HT, MT, LT, and VLT are the temperature ranges $155 > T > 32$ °C; $32 > T > -43.5$ °C; $-43.5 > T > -72.5$ °C, and $T < -72.5$ °C, respectively.

shows a complex functional dependence on temperature. In particular, in correspondence of the above-described temperature regions, the following conductivity behaviors are observed (Figure 8): (a) in the VLT region all the membranes show a single linear Arrhenius plot; (b) in the HT+MT+LT region one single VTF curve is observed for N117 and $[N117^{x-}(TEA^+)_x/(TEA\text{-}TF)_y]$; and (c) in HT+MT and MT+LT regions two different VTF curves are revealed for $[N117^{x-}(TEA^+)_x]$. In the HT, MT, and LT regions of $[N117^{x-}(TEA^+)_x/(TEA\text{-}TF)_y]$, $\sigma_{DC,1}$ is higher than that of other materials, thus indicating that TEA-TF embedded in the polar domains of Nafion facilitates the migration of the space charges present near the interfaces between the various phases. At $T > 5$ °C, after the melting of water traces, $\sigma_{DC,1}$ of $[N117^{x-}(TEA^+)_x]$ is higher than that of pristine N117. This observation points out that, in neutralized Nafion, the density of charges at the interfaces is higher than that of pristine N117, where in the presence of traces of water and owing to the easy dissociation of the sulfonic acid group a low surface concentration of protons is expected. At $T < 5$ °C, $\sigma_{DC,1}$ of $[N117^{x-}(TEA^+)_x]$ is lower than that of other membranes, thus indicating that the traces of water are essential to assist long-range charge transfer processes at the interfaces between the various phases. Furthermore, it is expected that, at temperatures lower than −72 °C, the conductivity occurs basically owing to hopping processes between neighboring sites at the interfaces between the nanophases. Pristine TEA-TF is the most conducting material and behaves differently from the other systems (Figure 8). TEA-TF, after melting at $T > 32$ °C, exhibits a VTF behavior for the bulk dc conductivity, while, at $T < 32$ °C, it presents two different Arrhenius-like behaviors which intersect at $T = 5$ °C. Table 2 reports the pseudoactivation energies for $\sigma_{DC,1}$ and $\sigma_{DC,2}$ profiles determined by fitting the above-described temperature regions by VTF or Arrhenius-like equations. It is to be observed that in the HT region N117 presents an $E_{\sigma_{DC,1}}$ value of 8.6 kJ·mol^{-1}, which is more than 1 order of magnitude higher than $E_{\sigma_{DC,2}}$. This evidence demonstrates that proton migration in N117 occurs owing to a conduction mechanism which is strongly dependent on the dynamics of water solvent. In the same temperature region the $E_{\sigma_{DC,2}}$ of $[N117^{x-}(TEA^+)_x/(TEA\text{-}TF)_y]$ is on the order of 1.75 kJ·mol^{-1}. This value is similar to that of pristine TEA-TF (1.37 kJ·mol^{-1}) and three times lower than that of $E_{\sigma_{DC,1}}$. The coincidence of $E_{\sigma_{DC,2}}$ values of $[N117^{x-}(TEA^+)_x/(TEA\text{-}TF)_y]$ and TEA-TF and the difference in energy barriers between $E_{\sigma_{DC,2}}$ and $E_{\sigma_{DC,1}}$ indicate that the long-range proton transfer in $[N117^{x-}(TEA^+)_x/(TEA\text{-}TF)_y]$ occurs predominantly with a mechanism strongly correlated to the charge migration processes which take place in TEA-TF. Furthermore, in the HT region, $[N117^{x-}(TEA^+)_x]$ presents a value of $E_{\sigma_{DC,2}} = E_{\sigma_{DC,1}} \approx 3.8$ kJ·mol^{-1}. This value is twice the values of $E_{\sigma_{DC,2}}$ of TEA-TF and $[N117^{x-}(TEA^+)_x/(TEA\text{-}TF)_y]$ and is approximately of the same order of magnitude of $E_{\sigma_{DC,1}}$ in the MT and LT regions of the $[N117^{x-}(TEA^+)_x/(TEA\text{-}TF)_y]$ membrane. Therefore, it is to be admitted that, at temperatures between the melting point (32 °C) and the T_c (−72.5 °C) of TEA-TF, the conductivity of the investigated membranes takes place with a similar mechanism, which involves the relaxation events of the polar side groups present at the interfaces of the bulk polymer. It is clear that these latter processes are dependent mainly on the segmental motion of fluorocarbon chains. At $T < -72.5$ °C, the $E_{\sigma_{DC,1}}$ of the studied membranes is higher than 10 kJ·mol^{-1}, thus suggesting that in the VLT region the charge migration occurs mainly owing to hopping processes.

Further insights into the conductivity mechanism of the membranes were determined by studying in detail the dependence on $1/T$ of the remaining fitting parameters determined by eq 1 on the BDS profiles shown in Figure 6 (see the available Supporting Information). The results of BDS studies indicate that in the explored temperature range $[N117^{x-}(TEA^+)_x]$ and $[N117^{x-}(TEA^+)_x/(TEA\text{-}TF)_y]$ conduct through two types of conductivity mechanisms. The first mechanism predominates at temperatures higher than 5 °C and is extensively correlated to the segmental motion of fluorocarbon backbone chains and to the structure and the interactions occurring between the polar side groups and the environment. The intensity and the density of these latter interactions depend on the structure of the side groups of the polymer host matrix and on the types of embedded low molecular aggregate components such as the interstitial traces of water and TEA-TF. The conductivity mechanism in this region seems to be in accordance with the peristaltic-like mechanism proposed previously for hybrid inorganic−organic composite Nafion membranes.[19,20,23] This mechanism hypothesizes that long-range charge transfer migrations occur successfully when two or more neighboring domains of water or TEA-TF contact each other owing to their shape and size modulations, which are triggered by the relaxation movements of the PTFE domains and of the side groups of the host N117 polymer. The second conductivity mechanism is responsible for the bulk conductivity at $T < 5$ °C. This phenomenon takes place owing to the presence of mobile space charges located at the interfaces between the various nanophases composing the membranes. These latter charges can easily migrate by hopping processes owing to the segmental motion and the side polar group relaxations of the host polymer. In particular, it was determined that segmental motion is predominant in the temperature range $5 > T > -72$ °C, while at $T < -72$ °C the relaxation of polar side groups plays a crucial role. In summary, at $T < 5$ °C charge migration in proposed bulk materials occurs due to a conductivity mechanism very similar to that typically observed in polymer electrolytes.[32,48] Taken together, in these conditions proton migration occur thanks to (a) the proton hopping processes between neighboring coordination sites mediated by segmental motions and relaxation processes of polar

Table 2. Pseudo-Activation Energies (E_x) Determined by Fitting VTF, VTFH, and Arrhenius-Like Equations to the Dependence on Temperature of $\tau_{DC,i}$ with $i = 1,2$ and Relaxation Times

Material	x	i	E_x / kJ·mol^{-1}			
			HT[a]	MT	LT	VLT
TEA-TF		1	1.37±0.04 [b]	84.4±0.3 [c]	51.53±0.08 [c]	-
N117	$\sigma_{DC,i}$	1	8.60±0.02 [d]			17.5±0.4 [c]
		2	0.54±0.01 [d]	-	-	-
	f_i	α	0.21±0.01 [b]			
		β		35.34±0.08 [c]		
		γ				94.0±0.4 [c]
[N117^{x-}(TEA$^+$)$_x$]	$\sigma_{DC,i}$	1	3.812±0.07 [d]		2.36±0.09 [d]	13.795±0.02 [c]
		2	3.78±0.01 [d]	-	-	-
	f_i	α	0.72±0.02 [b]			1.0±0.2 [d]
		β_1		57.6±0.2 [c]		18.2±0.1 [c]
		β_2		75.3±0.2 [c]		
		γ			20.96±0.09 [c]	
[N117^{x-}(TEA$^+$)$_x$/(TEA-TF)$_y$]	$\sigma_{DC,i}$	1	5.32±0.06 [d]			30.2±0.05 [c]
		2	1.75±0.02 [d]	-	-	-
	f_i	α	0.499±0.005 [b]			0.75±0.02 [b]
		β_1	1.78±0.02 [b]	50.3±0.4 [c]		25.4±0.1 [c]
		β_2		70.2±0.3 [c]		
		γ				19.4±0.1 [c]

[a] HT, MT, LT, and VLT are the temperature ranges $155 > T > 32$ °C; $32 > T > -43.5$ °C; $-43.5 > T > -72.5$ °C; and $T < -72.5$ °C, respectively. [b] Pseudoactivation energy determined by VTFH equation: $f_i = A_i \cdot e^{-E_{fi}/[R(T-T_{0,i})]}$. [c] Activation energy determined by Arrhenius equation: $\sigma_{DC,i} = A_{\sigma,i} \cdot e^{-E\sigma_{DC,i}/RT}$, $f_i = A_i \cdot e^{-E_{fi}/RT}$. [d] Pseudoactivation energy determined by VTF equation: $\sigma_{DC,i} = A_{\sigma,i} \cdot (T^{-1/2}) \cdot e^{-E\sigma_{DC,i}/[R(T-T_{0,i})]}$.

side groups and (b) the presence of TEA-TF ionic domains at the interfaces of membrane nanophases, which act to facilitate the hopping events. A further confirmation of the relevance of the above-described results is easily realized if we consider that when in bulk membranes water is replaced by ILs the following are expected: (a) a significant increase of the acceptor number (AN) due to the ammonium cation and (b) a decrease of both the donor number (DN) associated with TF anions and the dielectric constant in side dipolar domains of materials. It is well-known that these phenomena concur to decrease significantly the proton mobility in membranes. Fortunately, the high concentration of TEA-TF ionic nanoaggregates detected above and the correlated relaxation modes of the hosting polymer matrix act to compensate the above-described negative effects, which are responsible for the increase of the viscosity and the decrease of the permittivity in the bulk nanochannels of membranes. In summary, with respect to water, the presence in bulk membranes of TEA-TF nanodomains improves significantly the material properties owing to its interactions with the host material nanophases. These latter interactions facilitate the proton hopping phenomena between neighboring coordination sites owing to the cooperative dynamics of PCIL nanoaggregates characterized by morphologies which are flexible, easily modulated, and endowed with a lower DN ability. Thus, proton migration occurs owing to hopping events between TEA^+ ions bonding the $-SO_3^-$ groups of the N117 side groups — MTAs and MTAs−MTAs dynamic bridges.

4. Conclusions

In this report new proton-conducting materials based on Nafion neutralized with triethyl amine (TEA) and impregnated with a TEA-TF proton-conducting ionic liquid (PCIL) were synthesized by a new two-step protocol and studied. The materials, which are meant as promising PEM candidates for anhydrous operation in PEMFCs operating at $T > 120$ °C, were prepared taking into account the following considerations. As N117 is neutralized, its SRC widens. As the PCIL is incorporated in the bulk material, it acts as an efficient plasticizing component for N117 and increases the anhydrous proton conductivity of the membranes. In addition, the PCIL leakage from [N117^{x-}(TEA$^+$)$_x$/(TEA-TF)$_y$] is reduced owing to the expected exchange processes occurring between fixed and mobile ionic species. It is to be emphasized that TEA-TF species in mobile nanoaggregates are characterized by the same ionic species which are fixed in neutralized side groups of the N117 host matrix. The presence of $R-SO_3^- \cdots TEA^+$ side groups in [N117^{x-}(TEA$^+$)$_x$] and [N117^{x-}(TEA$^+$)$_x$/(TEA-TF)$_y$] improved the thermal stability of $R-SO_3^-$ groups as detected by TG studies and reduced the hydrophilic character of the membranes. Indeed, a low W.U. was measured, which decreases in the order N117 (26%) > [N117^{x-}(TEA$^+$)$_x$/(TEA-TF)$_y$] (11%) > [N117^{x-}(TEA$^+$)$_x$] (6%). MDSC studies confirmed these results and revealed that a decrease of crystallinity in hydrophobic fluorocarbon domains of N117 occurred owing to the neutralization and plasticization of the host polymer by TEA-TF. DMA revealed that in [N117^{x-}(TEA$^+$)$_x$] a significant improvement of mechanical properties in terms of storage modulus was reached with respect to pristine N117. In addition, in [N117^{x-}(TEA$^+$)$_x$/(TEA-TF)$_y$] the presence of embedded TEA-TF in bulk [N117^{x-}(TEA$^+$)$_x$] membranes modified significantly the mechanical properties of the resulting membranes, reducing the reciprocal steric hampering of neutralized side groups and increasing the plasticization effect in hydrophobic fluorocarbon domains of the N117 host matrix. Vibrational studies carried out by FT-IR and FT-Raman techniques indicated that the hydrophobic fluorocarbon PTFE domains of Nafion consist of a blend of chains with 10_3 and 15_7 helical conformations. In the proposed materials the 15_7 conformation predominates, while the concentration of 10_3 is constant and close to ∼12%. Therefore, no modulation of fluorocarbon chain composition in hydrophobic domains of materials occurred in bulk membranes due to the neutralization of N117 and its subsequent treatment with TEA-TF. Furthermore, Raman peaks diagnostic of the structure and of the interactions of the triflate anions of TEA-TF revealed that the TF anions, when they are incorporated in the membranes, have the tendency to aggregate in micelle-

like nanoclusters with the CF_3-tails forming their "core" and the sulfonate heads located on the surface of the nanoaggregates. The bending and stretching spectral features of H_2O allowed us to conclude that, with respect to Nafion, the polar domains of the studied membranes are more hydrophobic. The amount of water solvating the $R-SO_3^-\cdots{}^+H\,N\,R_3$ bridges is similar in both $[N117^{x-}(TEA^+)_x]$ and $[N117^{x-}(TEA^+)_x/(TEA\text{-}TF)_y]$ membranes. Water included in pristine TEA-TF is present mainly as bulk water, while in proposed materials it is solvating preferentially the $R\text{-}SO_3^-\cdots{}^+HNR_3$ bridges of N117 side groups. The studies of the electrical responses of the proposed materials by broad band dielectric spectroscopy (BDS) revealed the presence of two conductivity regions delimited at $T = 5$ °C. At $T \geq 5$ °C (HT region) the proton migration in pristine N117 is dependent on the dynamics of water, while in $[N117^{x-}(TEA^+)_x/(TEA\text{-}TF)_y]$ it is correlated to a charge-transfer mechanism assisted by the dynamics of TEA-TF moieties. It was revealed that the charge-transfer processes in both N117 and $[N117^{x-}(TEA^+)_x]$ are directly correlated to the segmental motion of fluorocarbon backbone chains, while in $[N117^{x-}(TEA^+)_x/(TEA\text{-}TF)_y]$ these events are modulated by the relaxation modes of both fluorocarbon backbone chains and side groups. At $T <$ 5 °C, the long-range charge transfer mechanism occurs owing to "ion hopping" processes which are modulated by the side group relaxations and by "interfacial polarization" relaxation phenomena. These latter are ascribed to the relaxation events responsible for the buildup of space charges near the interfaces delimitating the various nanophases composing the hybrid membranes. Results indicated that the σ_{DC} of investigated materials is equal to $\sigma_{DC,2}$ and $\sigma_{DC,1}$ at $T \geq 5$ and $T < 5$ °C, respectively. Furthermore, at $T \geq 5$ °C the SRC of pristine N117 is $5 < T < 105$ °C, while that of $[N117^{x-}(TEA^+)_x]$ and $[N117^{x-}(TEA^+)_x/(TEA\text{-}TF)_y]$ is $5 < T < 145$ °C. In addition, σ_{DC} at 145 °C presents values decreasing in the order $7.3 \times 10^{-3} > 6.1 \times 10^{-3} > 9.7 \times 10^{-4}$ S·cm^{-1} for $[N117^{x-}(TEA^+)_x/(TEA\text{-}TF)_y]$, N117, and $[N117^{x-}(TEA^+)_x]$ membranes, respectively. In conclusion, the improved thermal and mechanical stability of the $R-SO_3^-$ groups of N117 neutralized by TEA^+ cations, together with the low W.U. and the consequently limited role played by water in the proton conductivity mechanism, make the $[N117^{x-}(TEA^+)_x/(TEA\text{-}TF)_y]$ membrane an interesting material. Nevertheless, for practical application in PEMFCs operating under anhydrous conditions at $T > 100$ °C a further improvement of the conductivity of these membranes is required.

Acknowledgment. Research was funded by the Italian MURST project NUME of FISR2003, "Sviluppo di membrane protoniche composite e di configurazioni elettrodiche innovative per celle a combustibile con elettrolita polimerico" (Development of composite protonic membranes and innovative electrode configurations for polymer electrolyte membrane fuel cells). The authors appreciate the skillful experimental assistance of Dr. Sandra Lavina and Dr. Matteo Piga.

Supporting Information Available: Supporting Information reports the following: (a) a detailed description of the reagents, of the determination of water uptake and membrane reference conditions, and of the instruments and methods used in the experiments; (b) results discussed in Section 3 (Results and Discussion) which were omitted in the manuscript for the sake of brevity. This material is available free of charge via the Internet at http://pubs.acs.org.

JA906975Z